Characterization of Guided-wave Propagation in Composite Plates

Kalyan S. Nadella[a], Ken I. Salas [a] and Carlos E. S. Cesnik*[a]
[a] Dept. of Aerospace Engineering, University of Michigan, Ann Arbor, MI 48109, USA

ABSTRACT

The increasing use of composite materials in multiple engineering applications has emphasized the need for structural health monitoring (SHM) technologies capable of detecting, locating, and classifying structural defects in these materials. Guided wave (GW) methods offer an attractive solution for SHM due to their tunable sensitivity to different defects and their ability to interrogate large structural surfaces. The complications associated with the material anisotropy and directionality in composites result in an increased need for accurate and efficient simulation tools to characterize GW excitation and propagation in these materials. This paper presents a theoretical model based on three-dimensional elasticity to characterize GW excitation by finite-dimensional transducers in composite laminates. The theory uses an eigenbasis expansion for a bulk transversely isotropic material combined with Fourier transforms, the global matrix approach, and residue theory to find the displacement field excited by an arbitrarily shaped finite-dimensional transducer. Experimental results obtained in a cross-ply composite laminate are used to assess the accuracy of the theoretical solution.

Keywords: structural health monitoring (SHM), guided waves (GW), transducer design, composite materials.

1. INTRODUCTION

Polymer-based composite materials are becoming indispensible in modern industries such as aerospace, infrastructure and energy because of their ability to customize the physical properties in addition to high strength, light weight, directional stiffness, and long fatigue life. Because of the demand for composite materials, the development of accurate and viable structural health monitoring (SHM) methods to monitor for defects and ensure structural integrity is crucial. GW is an attractive solution for SHM in composites as they are able to travel long distances and are capable of propagating along the surface and through the thickness of a structure [1]. Most importantly, GW can be made sensitive to specific defects, in terms of both dimension and location, by careful control of the testing parameters. For instance, by appropriately selecting the testing frequency it is possible to selectively interrogate specific interfaces in a multilayered composite as originally demonstrated by Cawley and Guo [2]. In addition to detecting localized defects such as delaminations, GW are capable of providing an indication of the overall degradation state of the material. It is well known that damage in composites results from a combination of matrix cracking and fiber breaking, which have the macroscopic effect of reducing the effective stiffness of the structure. These changes could be quantified based on the ultrasonic wave speed inferred from an onboard network of actuators and sensors to assess the overall health state of the composite.

GW propagation in multilayered composites is significantly more complicated than in isotropic materials. Most studies consider the composite material as a homogenous orthotropic medium, which is an adequate assumption if the GW mode wavelength is larger than the fiber dimensions. Within this framework, the main complication for wave propagation arises from the directional dependence of the material properties resulting in a wave steering effect. In contrast to isotropic materials, the wave energy tends to concentrate along specific directions according to the stiffness of the particular composite under consideration. This phenomenon can manifest itself in different ways according to the GW excitation method used. If geometrically axisymmetric sources such as piezoelectric discs are used, the resulting GW field can be significantly directional. In the case of unidirectional laminates, it has been previously shown that this directionality prevents significant GW energy from propagating normal to the fiber direction. For directional piezocomposite transducers, it has been experimentally observed that the wave packet may not travel along the direction in which it was launched [3]. As a result of these complications, simulation tools capable of characterizing wave excitation and propagation are crucial for the development of effective SHM systems.

*cesnik@umich.edu; phone 734-764-3397; fax 734-763-0578

Health Monitoring of Structural and Biological Systems 2010, edited by Tribikram Kundu,
Proc. of SPIE Vol. 7650, 76502H · © 2010 SPIE · CCC code: 0277-786X/10/$18 · doi: 10.1117/12.847887

Downloaded from SPIE Digital Library on 13 Nov 2010 to 141.212.191.202. Terms of Use: http://spiedl.org/terms

Traditional numerical tools such as the finite element method are not efficient in modeling wave propagation in composites due to the large computational cost involved in resolving short wavelengths with small time increments. Alternative methods such as the spectral element method [4] and the local interaction simulation approach [5] [6]are better suited for these analyses and are particularly useful in modeling structures with complex geometries (such as stiffened panels and sandwich structures). An alternative approach can be considered by constructing semi-analytical models based on physical principles to characterize wave propagation in composite materials. These tools are particularly useful in identifying the influence of transducer parameters, such as geometry and construction, on the GW field excited in the structure. Most of the work towards semi-analytical models for GW propagation in composites has used modal expansions of the displacement field, generally combined with a discrete representation of the transducer loading. For instance, Moulin *et al*. [7] used a finite element representation of the transducer region coupled with a normal mode expansion to represent the GW field away from the source. Similarly, Velichko and Wilcox [8] developed a theory to model 3D displacements excited by finite sized transducers using only the dispersion relationship and mode shapes obtained from 2D analyses. An alternative modeling approach is possible by developing three-dimensional elasticity-based models where no kinematic assumptions are made regarding the through-thickness deformation of the substrate. These solutions rely on an expansion of the displacement field using the propagating eigenmodes for a three-dimensional transversely isotropic material. As a result, these solutions provide important physical insight into the testing parameters needed for SHM applications such as selective interface interrogation. Lih and Mal [9] developed a formulation based on this framework where the transducer was represented through point forces on the surface of the laminate, and a numerical procedure was used to solve the integrals resulting from the Fourier transform application. Raghavan and Cesnik [10] presented a related analysis where the transducer was represented as a continuous distribution of tractions and a rigorous procedure for the Fourier inversion was presented. This paper presents a theoretical model based on three-dimensional elasticity to characterize GW excitation and propagation by finite-dimensional transducers in composite laminates using the framework presented in [10]. The analysis is sufficiently general to consider an arbitrarily shaped transducer, but only a circular piezoelectric wafer is considered in the solution process. Following a description of the theoretical developments, a set of experiments is presented to support the accuracy of the results. These are based on laser vibrometer measurements in a cross-ply composite laminate to provide a validation in the space domain. A detailed analysis of the results is subsequently presented where the sources of error and accuracy of the solution are discussed. The paper concludes with a sample application of the theoretical model to support SHM system design, where the transducer dimensions that maximize and minimize the transmission of specific GW modes are obtained.

2. THEORETICAL FORMULATION

The theoretical derivation of the GW field excited by finite-dimensional transducers in multilayered composites involves several steps. The process begins with setting up the 3-D governing equations of motion for a bulk transversely isotropic material, which determines the propagating wave modes and displacement field in such a medium. This forms an eigenbasis for calculating the displacement field in a multilayered composite by using Fourier transforms and the global matrix approach [11]. The resulting transform integrals are solved using residue calculus [10] to obtain the displacements in the physical domain. Figure 1 presents a flowchart illustrating the solution procedure [12]. The following sections briefly describe each of these steps.

Downloaded from SPIE Digital Library on 13 Nov 2010 to 141.212.191.202. Terms of Use: http://spiedl.org/terms

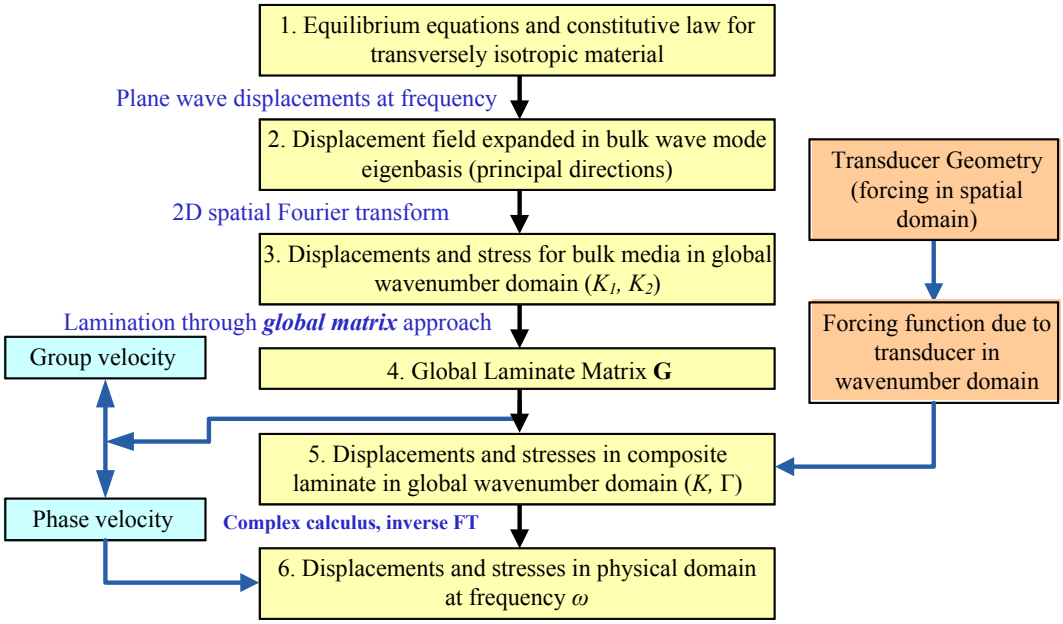

Figure 1. Theoretical formulation overview

2.1 Bulk Composite Medium

The analysis begins with the equilibrium equations for a transversely isotropic bulk medium in displacement form as:

$$\nabla \boldsymbol{c} \nabla^T \boldsymbol{u} = \rho \ddot{\boldsymbol{u}} \tag{1}$$

where $\boldsymbol{u}$ represents the displacement column vector, ρ represents the material density, and a double dot over a variable represents a double derivative with respect to time. The stiffness matrix $\boldsymbol{c}$ and the ∇ operator are defined as:

$$\boldsymbol{c} = \begin{bmatrix} c_{11} & c_{12} & c_{13} & 0 & 0 & 0 \\ c_{12} & c_{22} & c_{23} & 0 & 0 & 0 \\ c_{13} & c_{23} & c_{33} & 0 & 0 & 0 \\ 0 & 0 & 0 & c_{44} & 0 & 0 \\ 0 & 0 & 0 & 0 & c_{55} & 0 \\ 0 & 0 & 0 & 0 & 0 & c_{55} \end{bmatrix} \qquad \nabla = \begin{bmatrix} \frac{\partial}{\partial x_1} & 0 & 0 & 0 & \frac{\partial}{\partial x_3} & \frac{\partial}{\partial x_2} \\ 0 & \frac{\partial}{\partial x_2} & 0 & \frac{\partial}{\partial x_3} & 0 & \frac{\partial}{\partial x_1} \\ 0 & 0 & \frac{\partial}{\partial x_3} & \frac{\partial}{\partial x_2} & \frac{\partial}{\partial x_1} & 0 \end{bmatrix} \tag{2}$$

Defining ξ_1, ξ_2, and ζ to be wavenumbers along the x_1, x_2, and x_3 directions, respectively, for the bulk composite medium (corresponding to the principal material directions as shown in Fig. 2), and ω to be the angular frequency of harmonic excitation, the plane wave displacement field can be expressed as:

$$\boldsymbol{u} = \boldsymbol{\Omega}\, e^{-i(\xi_1 x_1 + \xi_2 x_2 + \zeta x_3 - \omega t)} \tag{3}$$

where $\boldsymbol{\Omega}$ corresponds to a 3 x 1 vector of constants. The displacement field obtained from Eq. (3) is substituted into the equilibrium equations defined in Eq. (1) to obtain an eigenvalue problem of the form:

$$\boldsymbol{B}\boldsymbol{\Omega} = 0 \tag{4}$$

where the matrix $\boldsymbol{B}$ is found by rearranging the equations of motion and is typically referred to as the Christoffel matrix for anisotropic materials[11]:

Downloaded from SPIE Digital Library on 13 Nov 2010 to 141.212.191.202. Terms of Use: http://spiedl.org/terms

$$\boldsymbol{B}=\begin{bmatrix} c_{11}\xi_1^2+c_{55}(\xi_2^2+\zeta^2)-\rho\omega^2 & (c_{12}+c_{55})\xi_1\xi_2 & (c_{12}+c_{55})\xi_1\zeta \\ (c_{12}+c_{55})\xi_1\xi_2 & c_{55}\xi_1^2+c_{22}\xi_2^2+c_{44}\zeta^2-\rho\omega^2 & (c_{23}+c_{44})\xi_2\zeta \\ (c_{12}+c_{55})\xi_1\zeta & (c_{23}+c_{44})\xi_2\zeta & c_{55}\xi_1^2+c_{44}\xi_2^2+c_{22}\zeta^2-\rho\omega^2 \end{bmatrix} \tag{5}$$

The resulting eigenvalue problem in Eq. (4) is solved for the through-thickness wavenumbers, ζ_i, in terms of the in-plane wavenumbers ξ_1 and ξ_2. These in-plane wavenumbers will be found for the entire laminate through the global matrix approach in a subsequent step in the analysis. ζ_1, ζ_2, and ζ_3 represent through-thickness wavenumbers for quasi-longitudinal, quasi-shear, and pure shear waves in the composite material, respectively. The positive root in each of these can be associated with upward traveling waves, while the negative root can be associated with downward traveling waves. These eigenvalues, along with their corresponding eigenvectors, can be used to express the displacement field as:

$$\boldsymbol{u}=\left(C_{1\mathrm{u}}\mathbf{e}_1e^{i\zeta_1x_3}+C_{2\mathrm{u}}\mathbf{e}_2e^{i\zeta_2x_3}+C_{3\mathrm{u}}\mathbf{e}_3e^{i\zeta_3x_3}+C_{1\mathrm{d}}\mathbf{e}_4e^{-i\zeta_1x_3}+C_{2\mathrm{d}}\mathbf{e}_5e^{-i\zeta_2x_3}+C_{3\mathrm{d}}\mathbf{e}_6e^{-i\zeta_3x_3}\right)\,e^{-i(\xi_1x_1+\xi_2x_2-\omega t)} \tag{6}$$

where the subscripts u and d are used to identify constants associated with upward and downward traveling waves, respectively. $C_{i\mathrm{u}}$ and $C_{i\mathrm{d}}$ (i= 1, 2, 3) are constants associated with upward and downward traveling waves, respectively. The vectors $\mathbf{e}_i$ (i =1, 2, 3) correspond to the through-thickness eigenvectors associated with $+\zeta_1$, $+\zeta_2$, and $+\zeta_3$, respectively. Similarly, the eigenvectors $\mathbf{e}_j$ (j =4, 5, 6) correspond to the through-thickness eigenvectors associated with $-\zeta_1$, $-\zeta_2$, and $-\zeta_3$. The resulting displacement field Eq. (6) can be represented in matrix form as:

$$\boldsymbol{u}=\begin{bmatrix}\boldsymbol{Q}_{11} & \boldsymbol{Q}_{12}\end{bmatrix}\begin{bmatrix}\boldsymbol{E}_u & 0 \\ 0 & \boldsymbol{E}_d\end{bmatrix}\begin{bmatrix}\boldsymbol{C}_u \\ \boldsymbol{C}_d\end{bmatrix}e^{-i(\xi_1x_1+\xi_2x_2-\omega t)} \tag{7}$$

to assist in global matrix formulation which will be presented in the next subsection. The following definitions have been employed in Eq. (7):

$$\begin{aligned} &\boldsymbol{Q}_{11}=[\mathbf{e}_1\quad\mathbf{e}_2\quad\mathbf{e}_3]\ ;\ \boldsymbol{Q}_{12}=[\mathbf{e}_4\quad\mathbf{e}_5\quad\mathbf{e}_6] \\ &\boldsymbol{E}_{\mathrm{u}}=\mathrm{Diag}[e^{i\zeta_1x_3},e^{i\zeta_2x_3},e^{i\zeta_3x_3}] \\ &\boldsymbol{E}_{\mathrm{d}}=\mathrm{Diag}[e^{-i\zeta_1x_3},e^{-i\zeta_2x_3},e^{-i\zeta_3x_3}] \end{aligned} \tag{8}$$

The expressions for these eigenvalues and eigenvectors can be found in Refs. [9,10]. At this point, the 2-D spatial Fourier transform (along the x_1 and x_2 directions) is introduced to facilitate the solution of the problem. This transformation takes the physical domain functions and replaces them with functions in the wavenumber domain, thereby facilitating the calculation of the strains and stresses due to the transform differentiation properties.

2.2 Multilayer analysis

From the solution of the displacement field for a transversely isotropic bulk medium (i.e., a single composite lamina), the global matrix approach introduced by Mal [11] is implemented to solve for the displacement field in a multilayered composite laminate. Due to the different orientations of the fibers in the composite layers, a global coordinate system (X_1, X_2, X_3) is introduced, which in general is not aligned with the local coordinate systems of the individual layers as shown in Fig. 2.

Downloaded from SPIE Digital Library on 13 Nov 2010 to 141.212.191.202. Terms of Use: http://spiedl.org/terms

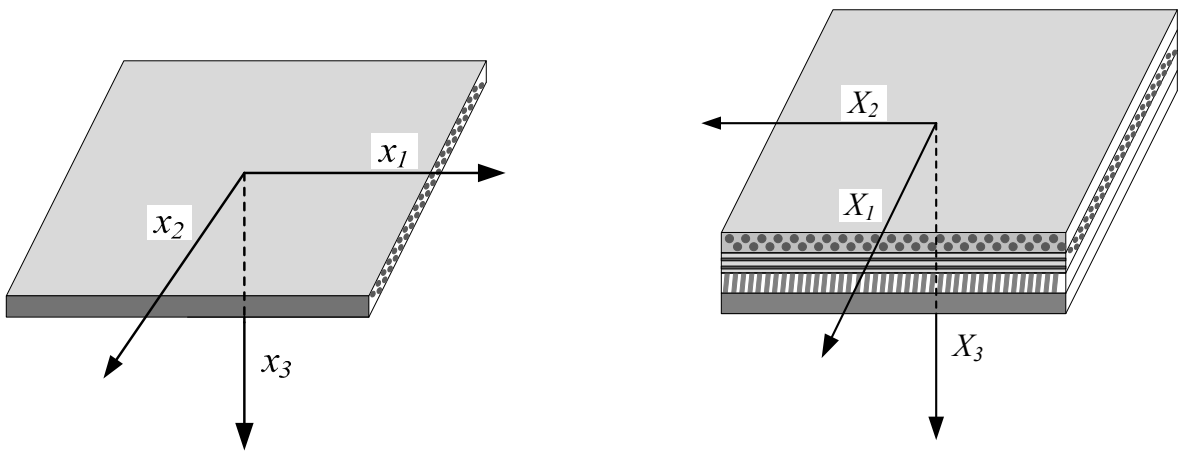

(a) (b)

Figure 2. (a) Transversely isotropic bulk medium with material coordinate axes (x_1, x_2, x_3) and fibers along the x_1 axis. (b) Composite laminate with plies oriented along different directions and laminate global coordinate system (X_1, X_2, X_3).

For a given m^{th} layer the material coordinate axis, x_1^m is aligned with the fiber direction, and all the local x_3^m axis are aligned with the global X_3 axis. As a result, the displacement vector **U** in the global system can be related to the displacement vector $\boldsymbol{u}$ in the local frame using a transformation matrix $\boldsymbol{L}^m$ defined as:

$$\boldsymbol{L}^m = \begin{bmatrix} \cos\varphi^m & \sin\varphi^m & 0 \\ -\sin\varphi^m & \cos\varphi^m & 0 \\ 0 & 0 & 1 \end{bmatrix} \tag{9}$$

where φ^m corresponds to the angle between x_1^m and global axis X_1. In order to conveniently implement the displacement and traction conditions between the layers of the laminate, a displacement-stress vector, **S**, of the following form is introduced:

$$\mathbf{S} = \begin{bmatrix} \mathbf{U} & \boldsymbol{\Sigma}_{i3} \end{bmatrix}^T \tag{10}$$

where **U** and $\boldsymbol{\Sigma}_{i3}$ correspond to the Fourier transform of the displacements and stresses, respectively. Therefore, the stress-displacement vector for the mth composite layer can be expressed as:

$$\mathbf{S}^m = \begin{bmatrix} \boldsymbol{L}^m & 0 \\ 0 & \boldsymbol{L}^m \end{bmatrix} \begin{bmatrix} \boldsymbol{Q}_{11}^m & \boldsymbol{Q}_{12}^m \\ \boldsymbol{Q}_{21}^m & \boldsymbol{Q}_{22}^m \end{bmatrix} \begin{bmatrix} \boldsymbol{E}_{\text{u}}^m & 0 \\ 0 & \boldsymbol{E}_{\text{d}}^m \end{bmatrix} \begin{bmatrix} \boldsymbol{C}_{\text{u}}^m \\ \boldsymbol{C}_{\text{d}}^m \end{bmatrix} = \boldsymbol{Q}^m \boldsymbol{C}^m \tag{11}$$

where $\boldsymbol{Q}_{21}^m$ and $\boldsymbol{Q}_{22}^m$ are matrices associated with the relevant interfacial stresses, and are dependent on the material properties and wavenumbers [11]. $\boldsymbol{E}_{\text{u}}^m$ and $\boldsymbol{E}_{\text{d}}^m$ shown in Eq. (11) are derived from $\boldsymbol{E}_{\text{u}}$ and $\boldsymbol{E}_{\text{d}}$ by changing the axis from local reference frame to the global reference frame.

$$\begin{aligned} \boldsymbol{E}_{\text{u}}^m(X_3) &= \text{Diag}\left[e^{i\zeta_1(X_3 - X_3^m)}, e^{i\zeta_2(X_3 - X_3^m)}, e^{i\zeta_3(X_3 - X_3^m)} \right] \\ \boldsymbol{E}_{\text{d}}^m(X_3) &= \text{Diag}\left[e^{-i\zeta_1(X_3 - X_3^m)}, e^{-i\zeta_2(X_3 - X_3^m)}, e^{-i\zeta_3(X_3 - X_3^m)} \right] \end{aligned} \tag{12}$$

Downloaded from SPIE Digital Library on 13 Nov 2010 to 141.212.191.202. Terms of Use: http://spiedl.org/terms

Using the global matrix approach, the displacement and stress continuity conditions at the interface between each layer can be enforced by using the matrix $\boldsymbol{Q}^m$ defined in Eq. (11). This procedure is explained in detail in Ref. [11]. Upon enforcement of the continuity conditions, a global laminate matrix, $\boldsymbol{G}$, is obtained from the individual $\boldsymbol{Q}^m$ which can be used in conjunction with the force vector, $\boldsymbol{F}$, to solve a system of the form:

$$\boldsymbol{GC} = \boldsymbol{F} \tag{13}$$

where $\boldsymbol{C}$ contains the $\boldsymbol{C}^m$ for the different layers that make the laminate. It must be noted that the laminate-level (global) in-plane propagating wavenumbers, K_1 and K_2, are obtained by seeking solutions for which the determinant of $\boldsymbol{G}$ becomes zero. The global in-plane wavenumbers are specific to each composite laminate and are related to the ply-level in-plane wavenumbers, ξ_1 and ξ_2, through a coordinate transformation using the rotation matrix $\boldsymbol{L}^m$. The global wavenumbers are then used to calculate the dispersion curves for the multilayered composite plate. In practice, this step is performed prior to the calculation of the constant vector $\boldsymbol{C}$. While this would result in a non-invertible system, a subsequent section will show that the singularity of the $\boldsymbol{G}$ matrix at these points is used in conjunction with the residue theorem of complex calculus to find the solution to the displacement field.

2.3 Piezo actuator forcing function

The force vector $\boldsymbol{F}$ introduced in the previous section depends on the excitation mechanism implemented. In this study, a circular piezoelectric wafer is used as the GW source. These devices are commonly used in the area of GW SHM due to their low cost and large bandwidth. The effect of the actuator on the substrate can be accurately represented by shear tractions along the edges of the transducer on the substrate's surface. This approach has been previously used by several researchers, and has resulted in accurate predictions of the excited GW field [10]. As a result, forcing functions f_1 and f_2 expressed in the global X_1 and X_2 axes, respectively, are introduced as shown in Eq. (10) to represent a circular piezoelectric wafer of radius R_O:

$$\begin{aligned} f_1 &= \tau_0 \delta(r - R_O)\cos\theta \\ f_2 &= \tau_0 \delta(r - R_O)\sin\theta \\ F_1 &= -i\tau_0 R_O J_1(KR_O)\cos\Gamma \\ F_2 &= -i\tau_0 R_O J_1(KR_O)\sin\Gamma \end{aligned} \tag{14}$$

where τ_0 represents the traction amplitude exerted by the transducer on the substrate, δ corresponds to the Dirac delta function, K corresponds to the radial in-plane wavenumber ($K = \sqrt{K_1^2 + K_2^2}$), J_1 corresponds to the Bessel function of the first kind, and Γ represents the azimuthal wavenumber ($\Gamma = \tan^{-1}(K_2 / K_1)$). The expressions in Eq. (14) also contain the Fourier transform of the forcing function (denoted as F_1 and F_2), which represents the entries of the vector $\boldsymbol{F}$ in Eq. (13). In the present study, the actuators are bonded on the top surface of the composite laminate, so that only the first two entries of the global force vector will be non-zero. After defining the forcing vector, the constants in Eq. (13) can be obtained from matrix inversion. Note that the solution for the system of equations is in the 2D Fourier domain, and the next section describes a Fourier inversion scheme to calculate the time domain displacement field in the physical domain.

2.4 Fourier inversion for global displacement field solution

In order to obtain the displacements in the physical domain, the inverse Fourier transform must be applied. This procedure results in the following expression for the displacement components u_j (j=1, 2, 3), evaluated at the surface where tractions are applied ($X_3 = 0$):

$$u_j = \int_0^{2\pi}\int_0^{\infty}\left[-\frac{\tau_0}{i\pi^2} R_O J_1(KR_O)\ \frac{\Psi_j(K(\Gamma),\Gamma)}{\Delta(K(\Gamma),\Gamma)} e^{-i[K(\Gamma) r\cos(\theta-\Gamma)-\omega t]}\right] K dK d\Gamma \tag{15}$$

where Ψ_j (j=1, 2, 3) is a function of the wavenumbers, composite layup, forcing function, and material properties, and Δ represents the determinant of the $\boldsymbol{G}$ matrix [10]. It is important to note that the radial wavenumber, K, is a function of the

Downloaded from SPIE Digital Library on 13 Nov 2010 to 141.212.191.202. Terms of Use: http://spiedl.org/terms

azimuthal wavenumber, Γ, due to the anisotropy of the material. The integrals in Eq. (15) are solved using residue calculus where the solution is expressed as a sum of the residues of the function Ψ/Δ. This part of the analysis is reproduced from Ref. [10], where the final result is shown to be:

$$u_j = \sum_{\hat{K}} \int_{\theta-\frac{\pi}{2}}^{\theta+\frac{\pi}{2}} \frac{-\tau_0}{2\pi} R_O [H_1^{(1)}(\hat{K}R_O) \pm H_1^{(2)}(\hat{K}R_O)] \frac{\Psi_j(\hat{K}(\Gamma),\Gamma)}{\Delta'(\hat{K}(\Gamma),\Gamma)} e^{-i\hat{K}(\Gamma) r \cos(\theta-\Gamma)} \hat{K} d\Gamma \tag{16}$$

and the term $\hat{K}$ represents the values of K for which the determinant of the $\boldsymbol{G}$ matrix becomes zero. As previously explained, these correspond to the propagating wavenumbers in the composite laminate. Similarly, $H_1^{(1)}$ and $H_1^{(2)}$ correspond to the Hankel function of first order and first and second kind, respectively. The term Δ′ represents the derivative of the determinant of $\boldsymbol{G}$ with respect to the wavenumber K evaluated at the propagating wavenumbers $\hat{K}$. Finally, the plus/minus sign refers to the fact that a positive sign must be used at all times except when $\cos(\theta - \Gamma) < R_O/r$.

3. EXPERIMENTAL PROCEDURES

3.1 Overview

Experiments were performed on 12-layer cross-ply $[0/90]_{3S}$ square plates with a side length of 0.5 m. These specimens were fabricated in an autoclave using IM7 carbon fibers and Cycom 977-3 resin from Cytec Engineered Materials [13] in unidirectional tape form, following the curing schedule indicated by the manufacturer. The mechanical characterization of the resulting composite was performed in two steps. Tensile tests on coupon-level specimens were conducted to determine basic elastic material properties along and normal to the fiber direction (E_1, E_2 and ν_{12}). The shear modulus G_{12} was calculated using ultrasonic measurements. In this approach, a sample specimen was instrumented with piezoelectric actuators and sensors and the wave speed of the fundamental antisymmetric mode along the fiber direction of the top layer was measured. The theoretical formulation described in the previous section was then used in conjunction with the mechanical properties obtained from tensile testing to find the value of G_{12} that matched the experimental wave speed. This approach is valid as the speed of this GW mode is predominantly dependent on G_{12}, as has been shown by previous researchers [14]. The value of G_{23} was obtained from the literature and additional efforts to characterize this parameter were not undertaken as it has a minor effect on the relevant GW speeds considered in this study [14]. The material properties used for the composite material system are summarized in table 1.

Table 1. Composite Mechanical Properties used in the analysis.

Mechanical Property	E_1	E_2	ν_{12}	G_{12}	G_{23}
Value	147 GPa	9.8 GPa	0.405	2.35 GPa	3.3 GPa

3.2 Experimental Setup

This section describes the experiments conducted to assess the accuracy of the theoretical solution. The composite laminate was instrumented with a 6.4-mm radius piezoelectric disc bonded at its geometric center for GW excitation. The input to the transducer was provided as a Hann-modulated toneburst with peak-to-peak amplitude of 300 V. The tests employed a Polytec PSV-400 scanning laser vibrometery[15] to assess the GW amplitude attenuation along different azimuthal positions in the composite laminate. These experiments were conducted at an excitation frequency of 75 kHz resulting in predominantly antisymmetric mode excitation. The experimental setup used is shown in Fig. 3(a) where the laser head is placed so that the out-of-plane velocity is measured. Figure 3(b) illustrates the retro-reflective tape that was placed on the surface of the composite to enhance the reflectivity of the material and optimize the laser visibility. Previous studies have shown that the presence of the tape does not affect the amplitude or wave speed of the propagating Lamb waves [3].The laser scan points consisted of multiple lines running through the center of the actuator. These lines were located at 0°, 30°, 45°, 60°, and 90°with 0° corresponding to the fiber direction of the top layer. Each grid line started at a distance of 20 mm from the center of the transducer and spanned until a distance of 85 mm from the center of actuator with a total of 92 points at each angle.

Downloaded from SPIE Digital Library on 13 Nov 2010 to 141.212.191.202. Terms of Use: http://spiedl.org/terms

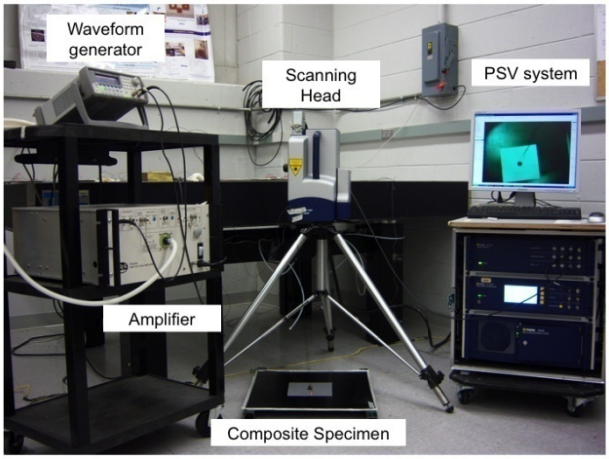

(a)

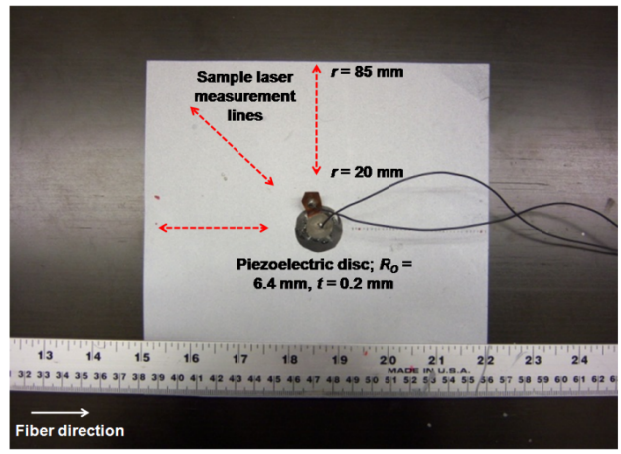

(b)

Figure 3. (a) Experimental setup showing different components used in the laser vibrometery experiments. (b) Picture of composite specimen with piezoceramic actuator along with retro-reflective tape

3.3 Radial Attenuation Characteristics

A critical aspect of GW interrogation of composites is the amplitude attenuation incurred due to geometric and material effects. Geometric effects are associated with the energy expansion through an increasing area, while material damping is associated with the viscoelastic matrix in the composite material. This section provides a comparison between the attenuation observed experimentally and that predicted by the theoretical model for various azimuthal directions in a cross-ply $[0/90]_{3S}$ laminate. As previously indicated, the present form of the theoretical formulation does not account for material damping effects although these can be included by using complex material constants. Therefore, the results will be useful in quantifying the relative attenuation due to material damping and geometric effects. Figure 4(a) shows the relative amplitude of the attenuation curve as a function of the azimuthal direction. The result indicates that the attenuation is similar for different angles, while the displacements amplitudes are larger along the principal material directions of the laminate (0° and 90°) which is expected based on wave steering considerations. A comparison between the experimental measurements and the simulation results are provided in Fig. 4(b) through Fig. 4(f). The experimental values reported correspond to the mean of two separate measurements while the error bars represent the associated standard deviation. As noted earlier, the amplitude of the displacements predicted by the theoretical model can be scaled by an arbitrary constant as the traction amplitude, τ_0, is unknown. In this case, this constant was selected such that the mean value in the displacement curve at each azimuthal position was equal for the experimental and theoretical data sets. The results show that the theoretical predictions are generally in good agreement with the experimental result, particularly as they mostly stay within the experimental uncertainty. Nevertheless, the overall rate of decay can be seen to be different particularly for the 30°, 45°, and 60° directions where the material attenuation is expected to be largest. These differences are associated with material damping. In order to quantify this effect, a power law curve was fitted to each experimental and theoretical curve (in the form $u = ar^b$, where r represents the distance from the source) and the results are summarized in table 2. Note that it has been generally reported in the literature that, for isotropic materials, geometric attenuation effects can be represented by such a power law with a power of -0.5. The results indicate that material damping effects can increase the wave amplitude attenuation by as much as 30% relative to geometric effects alone. This is observed to occur at an azimuthal angle of 60°. Furthermore, note that the lowest effect of material damping is observed along the fiber direction of the top layer. This result is expected as the fiber is the dominant phase along this direction.

Downloaded from SPIE Digital Library on 13 Nov 2010 to 141.212.191.202. Terms of Use: http://spiedl.org/terms

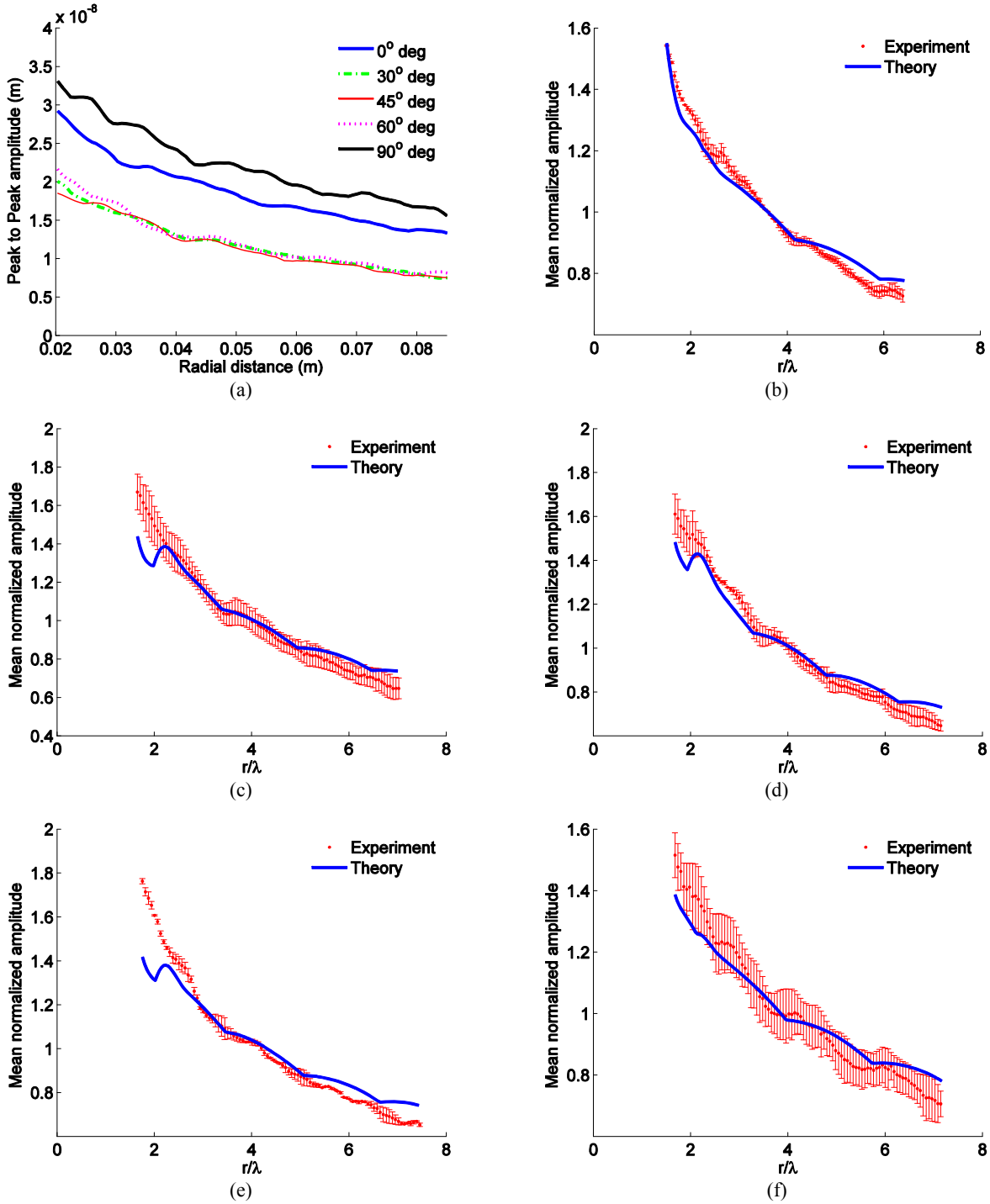

Figure 4. (a) Radial attenuation of the GW field induced by a circular piezoelectric wafer in the cross-ply laminate. (b)-(f) Comparison of mean normalized radial attenuation between theory and experiment in the cross-ply laminate $[0/90]_{6s}$ for azimuthal angles 0°, 30°, 45°, 60°, 90° respectively, r represents the distance from the source and λ the mode wavelength.

Downloaded from SPIE Digital Library on 13 Nov 2010 to 141.212.191.202. Terms of Use: http://spiedl.org/terms

Table 2. Summary of power law parameters used to characterize effect of material damping relative to geometric attenuation.

Angle (deg)	Experiment			Theory		
	a	*b*	R^2	*a*	*b*	R^2
0	0.21	-0.51	0.993	0.26	-0.44	0.993
30	0.14	-0.64	0.995	0.23	-0.48	0.961
45	0.14	-0.64	0.990	0.21	-0.51	0.982
60	0.13	-0.67	0.996	0.24	-0.47	0.977
90	0.21	-0.51	0.990	0.30	-0.39	0.995

3.5 Theoretical Model Application: Transducer Sizing

This section illustrates a sample application of the elasticity-based model developed in this study. A critical aspect in designing SHM systems is using a transducer that is sensitive to specific GW modes. This can be accomplished by selecting a transducer dimension that minimizes one mode while maximizing a different one. The theoretical model developed provides a fast tool to determine the transducer size needed for specific applications. In order to illustrate this, several parametric simulations were run where the transducer radius was varied. The out-of-plane displacement amplitude obtained under harmonic excitation was monitored at a fixed point and used as the metric to identify the effect of varying transducer dimensions.

Sample results are shown in Fig. 5 where the transducer radius has been normalized by the mode wavelength along each azimuthal direction. Note that by using this normalization most angles coalesce to a single curve implying that the ratio of radius to wavelength is the dominant parameter. It should be emphasized that such a curve can be used to select the desired sensitivity to any GW mode provided that the correct wavelength is selected. The reason for the behavior observed along the 30° direction is still being investigated. However, it is clear that transduction maxima are obtained with intervals of approximately 0.58 integer multiples of the wavelength while transduction minima are observed with intervals of approximately 0.85 integer multiples of the wavelength. The location of these points is associated with the roots of the Bessel and Hankel functions used in the analysis. In the case of an isotropic material, the result shown in Fig. 5 would be unchanged if plotted as a function of the transducer dimension alone. However, as discussed earlier, the GW mode wavelength varies with the angular position in composite materials due to the material anisotropy. As a result, the nominal dimension needed to obtain these maxima and minima will be different depending on the direction that is to be interrogated. This result is illustrated in Fig. 6 which shows that to maximize the displacements along the fiber direction of the top layer (0° direction), a transducer dimension that minimizes the sensitivity of that mode along its perpendicular direction must be selected.

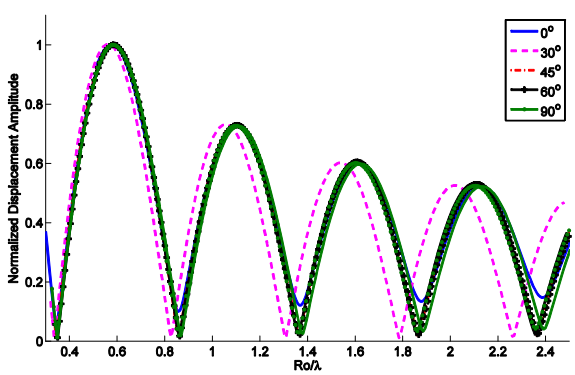

Figure 5. Effect of transducer radius on amplitude of induced GW field. Note that the radius normalization by the mode wavelength yields similar results for all azimuthal directions in the cross-ply $[0/90]_{3S}$ laminate, and that the results are valid for any frequency provided the correct physical wavelength is used.

Downloaded from SPIE Digital Library on 13 Nov 2010 to 141.212.191.202. Terms of Use: http://spiedl.org/terms

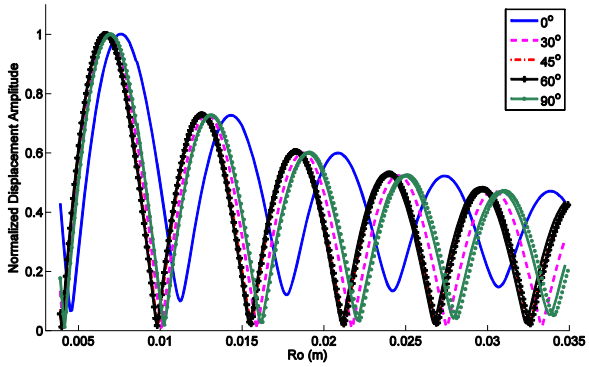

Figure 6. Effect of transducer radius on amplitude of induced GW field. Note that the nominal transducer dimension needed will be different for each azimuthal direction due to the spatial variation of elastic properties.

4. SUMMARY AND CONCLUSIONS

This paper presented a theoretical model based on 3-D elasticity to characterize guided wave (GW) propagation in composite laminated materials for structural health monitoring (SHM) applications. The analysis considered an eigenbasis expansion for a bulk composite medium combined with the global matrix approach and residue calculus to obtain the displacement field excited by a finite-dimensional piezoelectric transducer. The theoretical framework was applied to the case of GW excitation by circular piezoelectric transducers and the results were favorably compared with experimental measurements based on laser vibrometry in a cross-ply [0/90] laminate. In particular, it was shown that the GW amplitude attenuation was adequately captured as a function of propagation direction and distance. It was also indicated that the correlation can be improved by extending the geometric attenuation implicit in the theory to also consider material damping through complex material constants. Finally, the theoretical model was applied to identify the transducer dimensions needed to maximize and minimize the displacement the induced wave field. This analysis showed that different nominal transducer radii are needed to maximize the displacement field along different azimuthal directions in a composite laminate.

ACKNOWLEDGEMENTS

This work was supported by the NASA Constellation University Institutes Project/Advanced Composites Technologies Program under grant Z634001 with Thomas Acquaviva and Robert Draper as program managers.

REFERENCES

[1] Raghavan, A. and Cesnik, C.E.S., "Review of guided wave structural health monitoring," J. Vibration and Acoustics, 39(2):91-114 (2007).

[2] Guo, N. and Cawley, P., "The interaction of Lamb waves with delaminations in composite materials," Journal of the Acoustical Society of America, 94(4), 2240-2246 (1993).

[3] Salas, K.I. and Cesnik, C.E.S., "Guided wave structural health monitoring in composite materials using CLoVER transducers," Smart Materials and Structures, 19(1), 015014 (2010).

[4] Chakraborty, A., Gopalakrishnan, S., and Mahapatra, D.R., "Spectral finite element method," Springer (2007).

[5] Chaskelis, H.H., Delsanto, P.P. and Schechter, R.S., "Connection machine simulation of ultrasonic wave propagation in materials, II: the two-dimensional case," Wave Motion, 20(4), 295-314 (1994).

[6] Lee, B.C. and Staszewski, W.J., "Modeling of Lamb waves for damage detection in metallic structures: Part I. Wave Propagation," Smart Materials and Structures, 12(5), 804-814 (2003).

Downloaded from SPIE Digital Library on 13 Nov 2010 to 141.212.191.202. Terms of Use: http://spiedl.org/terms

[7] Moulin, E., Assaad, J. and Delebarre, C., "Modeling of Lamb waves generated by integrated transducers in composite plates using a coupled finite element-normal mode expansion," Journal of the Acoustical Society of America, 107(1), 87-94 (2000).
[8] Velichko, A. and Wilcox, P.D., "Modeling the excitation of guided waves in generally anisotropic multilayered media," Journal of the Acoustical Society of America, 121(1), 60-69 (2007).
[9] Lih, S.S. and Mal, A.K., "On the accuracy of approximate plate theories for wave field calculations in composite laminates," Wave Motion, 21(1):17-34(1995).
[10] Raghavan, A. and Cesnik, C.E.S., "Modeling of Guided-wave excitation by finite-dimensional piezoelectric transducers in composite plates," Proc. 47th AIAA SDM Conference, Honolulu, HI, Paper AIAA-2007-1725 (2007).
[11] Mal, A.K., "Wave propagation in layered composite laminates under periodic surface loads," Wave Motion, 10(3):257-266 (1988).
[12] Salas, K.I., Nadella, K.S. and Cesnik, C.E.S., "Characterization of guided-wave excitation and propagation in composite plates," Proc. 7th International Workshop on Structural Health Monitoring, Vol 1, Palo Alto, CA, pp 651-658 (2009).
[13] Anon., Cytec Engineered Materials IM7/Cycom 977-3 data sheet (2008).
[14] Vishnuvardhan, J., Balasubramaniam, K. and Krishnamurthy, C.V., "Genetic algorithm based reconstruction of elastic moduli of orthotropic plates using an ultrasonic guided wave STMR SHM array," Smart Materials and Structures, Vol. 16, Number 5, pp. 1639-1650 (2007).
[15] Anon., Polytec Scanning Laser Vibrometer, PSV 400 Hardware Manual, Polytec GmbH (2007).

Downloaded from SPIE Digital Library on 13 Nov 2010 to 141.212.191.202. Terms of Use: http://spiedl.org/terms